RUC

Roskilde University

Spring flood induced shifts in Fe speciation and fate at increased salinity

Herzog, Simon David; Conrad, S; Ingri, J; Persson, P; Kritzberg, E. S.

Published in:
Applied Geochemistry

DOI:
10.1016/j.apgeochem.2019.104385

Publication date:
2019

Document Version
Publisher's PDF, also known as Version of record

Citation for published version (APA):
Herzog, S. D., Conrad, S., Ingri, J., Persson, P., & Kritzberg, E. S. (2019). Spring flood induced shifts in Fe speciation and fate at increased salinity. *Applied Geochemistry*, *109*, Article 104385. https://doi.org/10.1016/j.apgeochem.2019.104385

General rights
Copyright and moral rights for the publications made accessible in the public portal are retained by the authors and/or other copyright owners and it is a condition of accessing publications that users recognise and abide by the legal requirements associated with these rights.

- Users may download and print one copy of any publication from the public portal for the purpose of private study or research.
- You may not further distribute the material or use it for any profit-making activity or commercial gain.
- You may freely distribute the URL identifying the publication in the public portal.

Take down policy
If you believe that this document breaches copyright please contact rucforsk@kb.dk providing details, and we will remove access to the work immediately and investigate your claim.

Download date: 04. Dec. 2025

Applied Geochemistry 109 (2019) 104385

Contents lists available at ScienceDirect

Applied Geochemistry

journal homepage: www.elsevier.com/locate/apgeochem

Spring flood induced shifts in Fe speciation and fate at increased salinity

S.D. Herzog[a,*,1], S. Conrad[b,1], J. Ingri[b], P. Persson[c], E.S. Kritzberg[d]

[a] Department of Science and Environment, Roskilde University, DK-4000, Roskilde, Denmark
[b] Department of Civil, Environmental and Natural Resources Engineering, Luleå University of Technology, SE-97187, Sweden
[c] Centre for Environmental and Climate Research & Department of Biology, Lund University, SE-223 62, Lund, Sweden
[d] Department of Biology/Aquatic Ecology, Lund University, SE-223 62, Lund, Sweden

ARTICLE INFO

Editorial handling by Michael Kersten

Keywords:
Fe geochemistry
Fe speciation
Fe isotopes
Organically complexed Fe
Fe (oxy)hydroxides
Boreal
Sub-arctic
Transport capacity
Salinity gradient
XAS

ABSTRACT

Rivers have traditionally been viewed as negligible sources of iron (Fe) to marine waters, as most Fe gets lost during estuarine mixing. However, recent findings demonstrate that Fe from boreal rivers display a higher resistance towards salinity-induced aggregation, presumably due to stabilizing interactions with organic matter. Previous studies have shown that Fe (oxy)hydroxides are selectively removed by aggregation processes, and that organic Fe complexes are less affected by increasing salinity. It has been further proposed that Fe speciation varies in response to seasonal differences in hydrology. In this study X-ray absorption spectroscopy (XAS) was used to determine the temporal variation in Fe speciation and the connection to Fe stability in response to increasing salinity in two boreal rivers (Kalix and Råne River), with the purpose to better understand the fate of riverine Fe export. Sampling was done from winter pre-flood, over the spring flood, to post-flood conditions (early April until mid June). In addition, parallel analyses for Fe speciation and isotope composition (δ^{56}Fe relative to IRMM-14) were made on river samples, as well as salinity-induced aggregates and the fraction remaining in suspension, with the main objective to test if δ^{56}Fe reflect the speciation of Fe.

The contribution of organically complexed Fe increased during spring flood compared to the pre- and post-flood, as did Fe transport capacity. However, since Fe (oxy)hydroxides were dominating throughout the sampling period, the seasonal variability was small. Interestingly, salinity-induced aggregation experiments revealed that Fe (oxy)hydroxides, which dominated aggregates, displayed lower δ^{56}Fe than in the river samples Fe, while organic Fe complexes in suspension had higher δ^{56}Fe values. The seasonal variability in Fe isotope signature could not be simply linked to Fe speciation, but was probably also influenced by variation in source areas of Fe and processes along the flow-path that alter both Fe speciation and isotopic composition.

1. Introduction

Despite the fact that Fe is one of the most abundant elements in the earth crust, Fe concentrations in the oceans are exceedingly low (Taylor, 1964). This is primarily due to the low solubility of Fe in oxic and nonacidic waters (Stumm and Morgan, 1996). As a micronutrient, Fe can be a limiting factor for primary production, since it is involved in key metabolic processes such as photosynthesis and cellular respiration (Sunda and Huntsman, 1997; Boyd and Ellwood, 2010). Further, due to the high surface reactivity of its mineral phases, Fe is tightly connected to biogeochemical cycles of e.g. C and P, by influencing their transport, bioavailability and sequestration in sediments (Lalonde et al., 2012; Lenstra et al., 2018).

Atmospheric deposition, hydrothermal vents, re-suspended sediment, pore water from continental shelves and riverine input are sources for Fe into the ocean (Tagliabue et al., 2017). Even if rivers can exhibit high Fe concentrations, riverine Fe has traditionally not been viewed as a significant source of bioavailable Fe to offshore marine waters (Jickells et al., 2005), as most Fe is lost by aggregation and sedimentation in estuarine salinity gradients (Sholkovitz, 1976; Chester and Jickells, 2003; Nowostawska et al., 2008). However, Fe from boreal rivers may exhibit surprisingly high stability to salinity-induced aggregation, and thus provide more Fe into the open sea than expected (Krachler et al., 2010; Kritzberg et al., 2014). This suggests that widely observed and rapid increases in Fe concentrations in north European freshwaters (Neal et al., 2008; Kritzberg and Ekstrom, 2012; Sarkkola et al., 2013; Weyhenmeyer et al., 2014; Björnerås et al., 2017) can result in increasing fluxes of Fe to marine waters.

* Corresponding author.
E-mail address: sherzog@ruc.dk (S.D. Herzog).
[1] Authors contributed equally.

https://doi.org/10.1016/j.apgeochem.2019.104385
Received 28 May 2019; Received in revised form 10 July 2019; Accepted 17 July 2019
Available online 22 July 2019
0883-2927/ © 2019 The Authors. Published by Elsevier Ltd. This is an open access article under the CC BY-NC-ND license (http://creativecommons.org/licenses/by-nc-nd/4.0/).

In river waters, two Fe carrying phases have been widely discussed - organically complexed mononuclear Fe (Fe-OM) and Fe (oxy)hydroxide complexes , often associated with chromophoric organic matter (Andersson et al., 2006; Breitbarth et al., 2010). It has been hypothesized that the fate of Fe in estuarine gradients is linked to these phases (Conrad et al., 2019). In line with that, previous work using direct assessment of Fe speciation by XAS, shows that the stability of riverine Fe is positively correlated to the relative contribution of Fe-OM complexes (Herzog, 2018), and that Fe (oxy)hydroxides are selectively lost by aggregation at increasing salinity (Herzog et al., 2017). Nevertheless, the fact that Fe-OM complexes were making a significant, albeit small, contribution also in aggregated fractions, illustrates that the degree of selectivity is complex (Herzog et al., 2017). Furthermore, in snapshot samples a higher contribution of Fe-OM complexes has been found during high discharge conditions in spring than during low discharge in winter (Herzog et al., 2019).

Temporal variation in river run off is closely connected to different hydro-geological pathways (Andersson et al., 2006; Neff et al., 2006; Pokrovsky et al., 2006). Weather events and hydrological seasonality impacts the residence time and pathways for soil and ground water and thereby affect geochemistry of river water (Dahlqvist et al., 2007; Ledesma et al., 2018). During winter, snow cover and frozen soil lead to a long residence time of groundwater, which promotes the formation of Fe(II). When this oxygen deficient groundwater enters the river, Fe (oxy)hydroxide will precipitate, and it is assumed to be the predominant form of Fe (Dahlqvist et al., 2007). In contrast, during high discharge episodes, sub-surface run off draining organic-rich soil layers, may provide a source for Fe-OM into the stream water (Dahlqvist et al., 2007; Grabs et al., 2012; Rosenberg and Schroth, 2017).

Several studies suggest that Fe isotopes can help distinguish between Fe-OM complexes and Fe (oxy)hydroxides (Ingri et al., 2006; Schroth et al., 2011; Ilina et al., 2013). The Fe isotope ratio is highly dependent on the oxidation state of Fe. When the redox state of an Fe phase changes between reduced and oxidized, the Fe(III) species tends to have a higher $^{56}Fe/^{54}Fe$ ratio than Fe(II) (Anbar et al., 2005). Fe isotope ratios appear to be influenced also by the source of riverine Fe, e.g. whether Fe originates from anoxic groundwater or organic rich soil layers (Escoube et al., 2015; Ingri et al., 2018). If Fe isotopes can be used to distinguish between Fe-OM and Fe (oxy)hydroxides, they could be used to reflect Fe speciation in marine waters, which is hitherto not possible by XAS, since the high concentration of salts and the low Fe concentration prevent isolation of enough Fe for the analysis. To assess what Fe isotopic composition reflects, a direct comparison with XAS analysis can be informative.

Knowledge about controls on Fe speciation and how it links to Fe transport capacity across estuarine salinity gradients is indispensable to better understand the consequences of increasing riverine Fe loading to the coastal regions and the open sea. This study aims to provide further information about seasonal variability in Fe speciation in river water to improve our understanding of how Fe is mobilized from source regions and transported into the ocean. More specifically, the research questions addressed are: 1) How Fe speciation, i.e. the relative contribution of Fe-OM complexes and Fe (oxy)hydroxides, vary from pre-flood to spring flood and post-flood conditions; 2) How this in turn affect Fe stability in response to increasing salinity; and 3) How Fe isotopic composition reflects Fe speciation.

To address these questions, the river mouths of two boreal subarctic rivers, Kalix River and Råne River, differing with respect to size, topography and land cover, were sampled from early March until mid-June to cover the main hydrological events. Riverine Fe was characterized for speciation (XAS), Fe isotope ratios (MC-ICPMS) and stability to increased salinity by artificial mixing experiments.

Fig. 1. The catchments of the boreal Kalix and Råne River, and their geographical position in Sweden (inset).

2. Materials and methods

2.1. Site description

The pristine, sub-arctic and boreal rivers Kalix and Råne have their origin in the Caldonian Mountains and the Råne Träsk, respectively. Both river catchments are located in Northern Sweden (Fig. 1) and consist mainly of forest, wetlands and lakes (Table 1). Additionally, the catchment of River Kalix is partly in the alpine area. The Quaternary deposits in this area are mainly glacial tills with well-developed podzol profiles (Fromm, 1965). The boreal forest is coniferous dominated by Norway spruce, Scots pine and birch (Nilsson and Wardle, 2005). The catchment of Kalix River is approximately 7 times larger than that of Råne River, whereas Råne River has more forest and wetland area than Kalix River (Table 1). The region has a sub-arctic climate and high seasonal temperature variations, with long cold winters and short, mild summers (Peel et al., 2007).

Between 40 and 50 % of the precipitation comes as snow and the

Table 1
Catchment and discharge information for Kalix and Råne River.The data in this table are provided by the Swedish Meteorogical and Hydrological Institute (SMHI) and are freely available at (www.vattenwebb.smhi.se).

	Kalix River	Råne River
Size (km^2)	28 113	4 207
Forest (%)	54.4	71.9
Wetland (%)	15.5	23.8
Mountain (%)	10.6	0.0
Lakes (%)	5.5	3.8
Others* (%)	14.0	0.5
Discharge (m^3/s):		
Maximum (12.05.2016)	1 830	484
Average Jan. to March (pre-flood)	96	17
Average May (spring flood)	1 093	254
Average June (post-flood)	589	52

* Grassland, heathland, beach, areas with low vegetation and fire field.

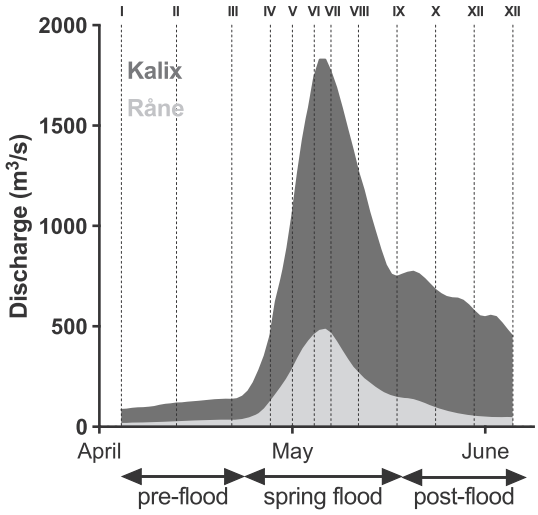

Fig. 2. Discharge in Kalix and Råne River during sampling period in 2016 (SMHI). The dashed lines and roman numbers indicate the samplings occasions (I - XII). The arrows below the x-axis denote pre-flood, spring flood and post-flood periods.

catchments and rivers are snow- and ice-covered from late November to April (Ingri et al., 1997). With 5–7 months of winter, the moisture in the soils and subsoils freezes down to a depth between 25 and 79 cm (Öquist and Laudon, 2008; Haei et al., 2010). Most of the snow and ice melts in May, and cause the discharge in both rivers to increase tremendously. During this transient event – the spring flood – discharge is elevated between 12 and 29 times in Kalix River and 14 to 47 times in Råne River (data from 2000 to 2017, SMHI).

2.2. Sampling and standard analytical methods

The sampling stations on the Kalix River (Kamlunge rapids) and Råne River (Orrbyn) were partly ice-covered until early May. Samples were collected at 12 occasions from early April until mid June to encompass conditions during pre-, spring, and post-flood (Fig. 2). Samples were collected from a bridge in the middle of the rivers. All sampling equipment was metal-free, acid-washed, and rinsed with ultrapure water (Milli-Q®). Subsamples were filtered through a 150 µm mesh and used for artificial seawater mixing experiments, and analysis of oxygen isotopes, total Fe and DOC concentrations. An additional 1 L volume of 150 µm filtered water was frozen as soon as possible and never more than 2 h after collection. This volume was later freeze-dried and stored dry and dark until characterized for Fe speciation (XAS) and Fe isotopic composition. Oxygen and pH were measured *in situ* with a Hydrolab Multisonde M5.

An ICP-AES Optima 3000DV (PerkinElmer) was used to determine total iron (tFe) concentration. Dissolved organic carbon (DOC) was analyzed by high temperature catalytic-oxidation on a Shimadzu TOC V-CPN analyzer, using the Non-purgeable Organic Carbon (NPOC) method. Salinity was determined by a WTW ninoLab Cond730.

Only acid washed material was used for sample handling and in addition, for XAS and total Fe analysis polycarbonate bottles/containers and spatula were used exclusively.

2.3. Artificial seawater mixing experiments

Mixing experiments to assess the Fe transport capacity - the fraction of riverine Fe remaining in suspension at increased salinity - were initiated as soon as possible, and no later than 2 h after sampling. For this purpose, river water samples were mixed with artificial sea salt solutions in a 6:1 ratio (vol:vol) to a total volume of 50 ml. Final salinities were 7 and 20, representative of the Baltic Proper and Kattegat respectively. An artificial sea salt stock solution was produced using reagent grade salts following a standard protocol (Kester et al., 1967), (mass fraction given in %: Cl^- (55.05), Na^+ (30.62), SO_4^{2-} (7.68), Mg^{2+} (3.69), Ca^{2+} (1.15), K^+ (1.10), HCO_3^- (0.40), Br^- (0.19), H_3BO_3 (0.07), Sr^{2+} (0.04), F^- (0.003)) to produce a salinity of 245. All chemicals used were reagent grade from Sigma Aldrich. The stock solution was diluted to the desired concentration with milli-Q water. After mixing the river water with the salt solution, the samples were stored in the dark on a shaker for 24–48 h to allow aggregation. The aggregates were then separated by centrifugation at 3000 *g* for 8 h at 4 °C. After centrifugation total Fe, DOC, pH and salinity were measured in the supernatant. The Fe transport capacity was calculated by dividing the Fe concentration in supernatant by the Fe concentration of the river samples multiplied by 100 (%).

$$FeTC = \frac{Fe_{supernatant\ at\ given\ salinity}}{Fe_{\text{river water}}} \times 100 \quad (1)$$

To be able to separate salinity-induced aggregates for characterization of Fe speciation and Fe isotopic composition, similar experiments were carried out with larger volumes – 5 L. The aggregated fraction was separated in three sequential centrifugation steps. In a first step samples were centrifuged at 4271 g for 1.5 h at 4 °C removing around 90 % of the total volume as supernatant. In a second and third step, the remaining supernatant was separated from the aggregated fraction by centrifugation (2516 g for 15 min at 4 °C). The aggregated fractions were frozen and freeze-dried. All freeze-dried samples were stored dry in the dark until analyzed by XAS and MC-ICP-MS.

2.4. XAS data collection and analysis

Freeze-dried river water samples and aggregates from salinity experiments were analyzed by XAS. XAS data was collected at beam line 4-1 at the Stanford Synchrotron Radiation Lightsource (SSRL), California, USA. SSRL was running in a top-up mode at 3.0 GeV beam energy and at ca. 500 mA ring current. The beam line was equipped with a Si[2 2 0] double crystal monochromator. Further, three consecutive ion chambers, to monitor the transmitted beam, and one passivated implanted planar silicon (PIPS) detector for fluorescence measurements were used. To reduce higher order harmonics the monochromator at 4-1 was detuned (50 %). Fe K-edge spectra were collected in a k-range up to 14 $Å^{-1}$ in a fluorescence mode. To reduce unwanted scattering and fluorescence contribution a Mn filter and Soller slits were used. Samples were mounted on a liquid nitrogen cryostat for measurements (ca. 80 K), to prevent beam-induced damage. The samples were aligned at 45° with respect to the incident beam. Depending on the Fe concentration 2 to 6 scans were recorded for each sample. Simultaneously, the spectrum of an Fe reference foil (Fe(0)) was recorded, to allow internal energy calibration.

Extended X-ray absorption fine structure (EXAFS) spectra and wavelet transform (WT) contour plot data treatment and analysis were performed according to Herzog et al. (2017). Through comparison of the edge position of the first derivate spectra of consecutive scans, all spectra were checked for beam damage and none were found. The scans were energy calibrated by setting the first inflection point of Fe(0) to 7111.08 eV (Wilke et al., 2001) and averaged by using SixPack (Webb, 2005). By comparing fluorescence and transmission data in Viper (Klementiev, 2000) self-absorption was investigated and in a few cases self-absorption was detected. These were corrected, using the formalism in Viper. The same program was used to normalize and subtract the background from all averaged spectra in order to isolate the EXAFS oscillations. The resulting k^3-weighted spectra were then fitted in k-space (3–12 $Å^{-1}$) with theoretical phase and amplitude functions calculated by the *ab initio* code FEFF7 (Zabinsky et al., 1995). Input structures used in the FEFF calculation were those of goethite (O'day et al., 2004) and the trisoxalatoiron(III) complex (Persson and Axe, 2005). While fitting, the threshold energy (ΔE_0) was varied but

correlated so that it was identical for all shells. Correlating coordination numbers and fixed Debye−Waller factors (σ^2) to values found in the literature, restricted the number of free variables. In all refinements, the amplitude reduction factor (S_0^2) was set to 0.898, which is close to recommended values (Ankudinov et al., 1992) yielding a first-shell Fe-O coordination number close to six in the vast majority of the samples. EXAFS data was further analyzed by wavelet transform (WT), following the procedure described by Karlsson and Persson (2010). The program WT Igor Pro script developed by Funke et al. (2005) was used to qualitatively differentiate between different backscatters (Funke et al., 2005; Karlsson et al., 2008).

A linear combination fitting (LCF) analysis was applied to estimate the proportions of various Fe phases in the samples. LCF was performed on the k^3-weighted EXAFS spectrum in the k range from 3.0 to 12.0 $Å^{-1}$. For the LCF fitting, model compounds spectra from ferrihydrite, lepidocrocite, biotite goethite, magnetite, hematite, augite and Fe(III) complexed to Suwannee Rives fulvic acid were used as references. In this analysis, E_0 was allowed to float, non-negative boundary condition was used and the sum was not forced to equal 1. All components with a contribution of < 10 % were excluded from the results.

The normalized X-ray absorption near edge structure (XANES) spectra and the corresponding first derivative spectra were qualitatively compared using SixPack. Further oxidation state analysis from pre-edge information was performed according to Wilke et al. (2001). The data pre-treatment was accomplished using the XANES dactyloscope software (Klementiev, 2002), and the baseline corrected pre-edge was fitted with two pseudo-Voigt functions (50 % Gaussian and 50 % Lorentzian) using Fityk (Wojdyr, 2010). This yielded the pre-edge intensity and the pre-edge centroid energy.

2.5. Isotopic composition

Fe isotopic compositions were measured at ALS Scandinavia AB. High purity Suprapure® acids were used throughout sample treatment. For the Fe isotope ratio measurements, freeze-dried river water samples and the aggregates from the aggregation experiment were re-dissolved in 1 mL 9 M HCl. Iron was separated from the matrix by ion exchange, with a recovery > 95 %. The Fe isotope compositions in the separated fractions were measured using a Multi Collector Inductively Coupled Plasma Mass Spectrometer (MC-ICP-MS, NEPTUNE PLUS®, Thermo Scientific) equipped with micro-concentric nebulizer and tandem cyclonic/Scott double pass spray chamber. Instrumental mass biases were corrected by sample-standard bracketing using IRMM-14 CRM, while an internal standard (Ni) was added to all samples and used to correct for instrumental drift (Baxter et al., 2006). Each sample was measured twice with the sample-standard bracketing method and both δ^{56}Fe and δ^{57}Fe data are reported in the supplement (Equations (2) and (3), respectively). Fe isotope data were reproduced with a precision of 2.7 % (n = 7). Blanks, in-house and geological reference material were processed and analyzed with the samples to assure quality and exclude potential fractionation processes.

$$\delta^{56}Fe(‰) = \left[\frac{(\,^{56}Fe/\,^{54}Fe)_{sample}}{(\,^{56}Fe/\,^{54}Fe)_{IRMM-14}} - 1 \right] * 10^3 \quad (2)$$

$$\delta^{57}Fe(‰) = \left[\frac{(\,^{57}Fe/\,^{54}Fe)_{sample}}{(\,^{57}Fe/\,^{54}Fe)_{IRMM-14}} - 1 \right] * 10^3 \quad (3)$$

Oxygen isotopes (δ^{18}O) were measured with a Liquid Water Isotope Analyzer (LWIA) at the stable isotope lab (SIL) at the department of geological sciences at Stockholm University. The LWIA provides isotope ratio measurements by laser absorption spectroscopy (off-axis integrated cavity output spectroscopy).

2.6. Statistics

The F-test was applied to statistically verify the contributions from scattering paths to higher coordination shells in the EXAFS fits (Klementev, 2001). As a relative estimate of the contribution of the Fe-OM and Fe (oxy)hydroxides within the river samples and aggregates, a ratio between the two species was calculated from the XAS results. Two different measures were used: 1) the quotient between the coordination numbers of the Fe-C path and the short (edge-sharing) Fe-Fe path; 2) the quotient between the Fe-OM fraction and the sum of Fe-oxides fractions from the LCF results. Differences in the relative distribution of Fe-OM and Fe (oxy)hydroxide between river water samples and the aggregated samples (as assessed by LCF) were tested by paired t-tests. Relationships between variables (e.g. XAS results, Fe and O isotopes, Fe transport capacity) were tested by Pearson correlations. Assumptions of normality were verified by Shapiro-Wilk test.

3. Results

3.1. Seasonal variation

Discharge increased in late April and peaked in mid-May with a maximum of 1830 and 484 m^3/sec in Kalix and Råne River, respectively (Fig. 2). After a couple of weeks, the spring flood discharge declined to the base flow level (post-flood) in Råne River, whereas the drop in discharge was less pronounced in Kalix River (Fig. 1). Oxygen was saturated in both rivers (95–106 %) during the sampling period.

The DOC concentration showed a similar range during the spring flood, but was lower for Kalix River during pre- and post-flood, while tFe was consistently higher in Råne River (Fig. 3 a and b). Total Fe concentration increased from pre-flood conditions and reached a maximum just before spring flood and then declined to levels lower than during pre-flood. A drop in pH, conductivity and in δ^{18}O during the peak of the spring flood was recorded for both rivers (Fig. 3 c, d e and f). During post-flood all variables recovered to close to pre-flood levels, though conductivity remained low in Råne River. Correlation statistics of the variables mentioned in this paragraph (tFe, DOC, pH, O isotopes and conductivity) can be found in the supporting information (SI) for Kalix River and for Råne River (Table S1).

XAS analysis identified Fe (oxy)hydroxide and Fe-OM complexes in the river water samples of Kalix and Råne. The Fe (oxy)hydroxide signal was dominating strongly in all river samples. A slight seasonal variation in the contribution of Fe-OM complexes was detected. The WT intensity of the light back-scattering at low k-values, representing Fe-OM complexes, increased during spring flood, followed by a decrease during post-flood as shown by the selection of WT plots in Fig. 4; WT plots of all measured samples are shown in the SI in Fig. S1.

EXAFS fitting confirmed the presence of both Fe phases in all samples. Comparison of the CN-ratios among the samples revealed a variation in the relative contribution of the Fe species ($CN_{Fe\text{-}C}/CN_{Fe\text{-}Fe}$, Fig. 3 g and h and Table S2). The CN-ratio, indicative of the relative contribution of Fe-OM, increased with discharge during the spring flood with a distinct drop during peak discharge, followed by declining values during post-flood conditions. The LCF analysis identified a mixture of Fe oxides and Fe-OM complexes. Three components were dominating in all samples, ferrihydrite, Fe(III) complexed to natural organic matter, and lepidocrocite (Fig. S2). The LCF ratio (the ratio between the Fe-OM fraction and the sum of the ferrhydrite and lepidocrocite; Fig. 3 in plot g and h) was strongly correlated with the $CN_{Fe\text{-}C}/CN_{Fe\text{-}Fe}$ ratio (Table 2). Fe speciation (CN-ratio and LCF-ratio) showed no significant correlation with any other measured variable ($p > 0.70$).

Analysis of the XANES region revealed uniform results among all river samples (Fig. S3 a). The double peak of the first derivative XANES spectra detected in all samples (Fig. S3 b) was indicative of a strong contribution from Fe (oxy)hydroxides (Sundman et al., 2014). Furthermore, the pre-edge analysis based on the procedure of Wilke et al.

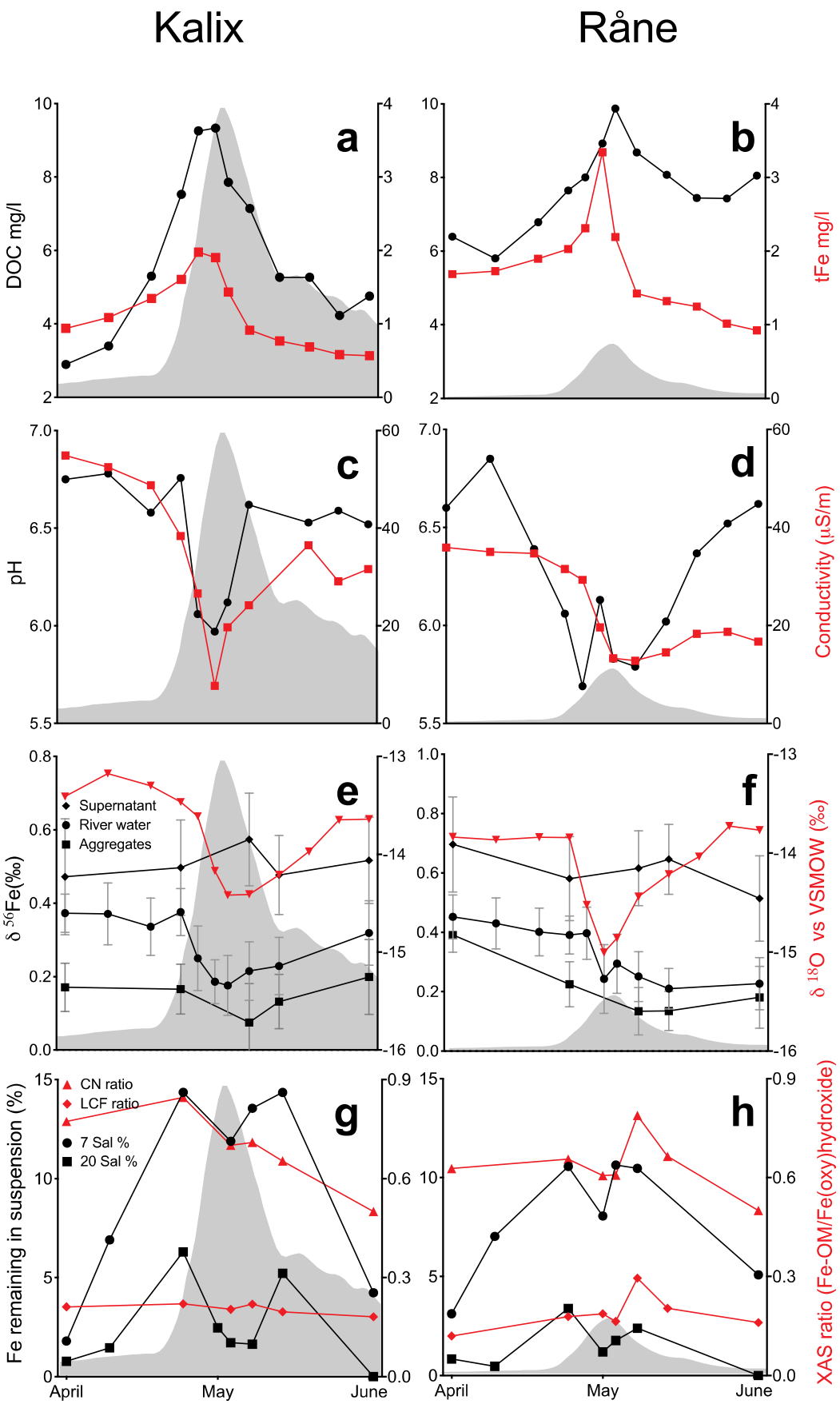

Fig. 3. Variation in water chemistry over the sampling period in Kalix (left) and Råne River (right). Panels show DOC and tFe (a and b), pH and conductivity (c and d), δ^{56}Fe of river water samples, aggregates and supernatant (error bars ± 2σ) and δ^{18}O vs VSMOW (e and f), and Fe transport capacity at salinity 7 and 20 and the CN and LCF ratios (g and h). The grey area represents discharge.

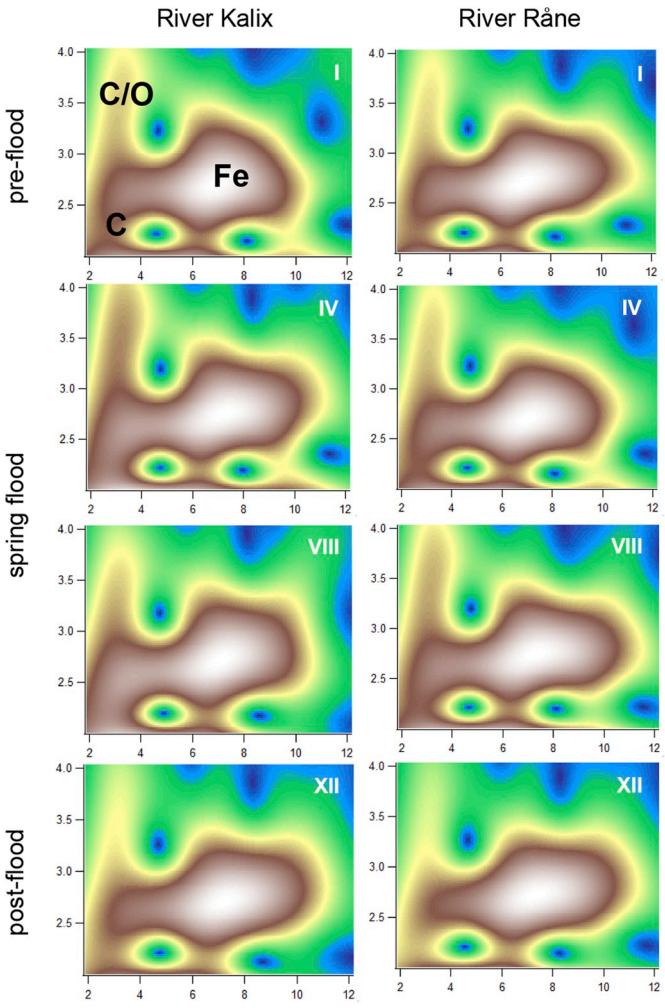

Fig. 4. High resolution WT counter plots (η = 8, σ = 1) of EXAFS data of a selection of river water samples from Kalix River (left) and Råne River (right). The sampling occasions are indicated with roman numbers: I (05.04.16), IV (02.05.16), VIII (25.05.16) and XII (15.06.16) and are associated to pre-, spring and post-flood. In the upper left plot the areas representing the different Fe paths are denoted by C for the Fe – C path, C/O for the multiple scattering path Fe – C – C/O, and Fe for the two Fe – Fe paths.

Table 2
Correlation coefficients of the artificial seawater mixing experiments for Kalix and Råne River for a selection of variables. A complete overview of the statistics can be found in the SI (Table S1).

Variable 1	Variable 2	Kalix River		Råne River	
		r	p	r	p
Fe transport capacity (sal7)	DOC	0.80	0.029		
Fe transport capacity (sal7)	pH			−0.82	0.025
Fe transport capacity (sal 20)	pH			−0.76	0.047
Fe transport capacity (sal 20)	CN ratio	0.53	0.276	0.70	0.126

(2001) indicated a predominance of Fe(III) as seen in Fig. S4. The centroid pre-edge energies of the all samples showed almost no variation (7113.6–7113.7 eV), and the intensities remained constant at a value in agreement with predominantly 6-coordination (Fig. S3). For more information on the XAS results see SI (Figs. S1, S2, S4 and Table S2).

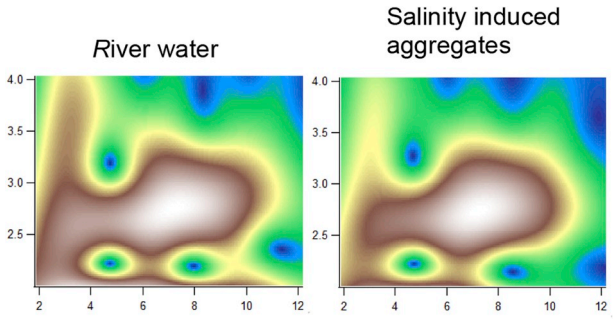

Fig. 5. High resolution WT modulus (η = 8, σ = 1) of EXAFS data of a river water sample from the sampling event River Kalix IV (02.05.16) and the corresponding salinity induced aggregates at salinity 7, plotted as a function of k (Å − 1) on the x-axis and R (Å) on the y-axis.

3.2. Fe at increasing salinity

A major loss of Fe from suspension was observed in response to increasing salinity – Fe transport capacity at salinity 20 was never above 7 % (Fig. 3 g and h). For both rivers and both salinities the Fe transport capacity increased with increasing discharge and dropped during peak flow, but recovered temporarily and then declined with declining discharge. Fe transport capacity in Kalix River correlated with DOC at salinity 7 and Fe transport capacity in Råne River correlated negatively with pH (Table 2). No correlation was found between the Fe transport capacity and Fe speciation (CN- and LCF-ratio) (Table S1).

The XAS results showed that the Fe (oxy)hydroxide contribution dominated in all aggregate samples from both rivers (Fig. 5). Comparison with the river water samples indicated a selective removal of Fe (oxy)hydroxides with increasing salinity (Fig. 5), i.e. the CN-ratios determined for the aggregated samples were significantly lower than the corresponding river water samples (t_5 = 9.403; p < 0.001) (Table S2). Also, the fraction of Fe-OM complexes in the aggregates as determined by LCF was lower than in the corresponding river water samples (t_5 = 5.625; p = 0.005) (Table S3 – Table S6). The XANES results for the aggregated samples showed a predominance of Fe(III), similar to the river water samples (Fig. S3).

3.3. Fe isotopic composition

Fe isotopes were measured on river water samples, and the aggregates and supernatant produced by enhanced salinity. All measured δ^{56}Fe ratios were positive relative to IRMM-14. River water δ^{56}Fe values of Kalix and Råne River decreased with increasing discharge during the spring flood. In Kalix River the δ^{56}Fe value gradually increased as discharge declined, whereas in Råne River the δ^{56}Fe value remained low. River water δ^{56}Fe correlated with discharge and δ^{18}O in Kalix River, and with DOC and conductivity in both rivers (Table S1).

The δ^{56}Fe ratios of the aggregates were consistently depleted in the ^{56}Fe isotope compared to the river water samples, whereas the Fe in the supernatant was consistently enriched in the ^{56}Fe isotope (Fig. 3 e and f). The δ^{56}Fe values of the aggregates in both rivers ranged from 0.08 ± 0.11 to 0.39 ± 0.06 ‰, and the δ^{56}Fe of the supernatant ranged from 0.47 ± 0.16 to 0.70 ± 0.16 ‰ (Table S8). Overall, the Fe isotope composition in Råne River was slightly more positive than in Kalix River. The temporal dynamics of δ^{56}Fe of the aggregates follow those of the river water samples.

4. Discussion

4.1. Seasonal variation of Fe speciation

The spring flood caused by the snowmelt is the major hydrological event in Kalix and Råne River and has a major impact on the water

chemistry. The temporal dynamics suggest that variation in the hydro-geological pathways is strongly influencing water chemistry, which has been observed in previous studies (Dahlqvist et al., 2007; Rosenberg and Schroth, 2017). The low Fe and DOC concentrations, high pH and conductivity, and heavy $\delta^{18}O$ values found during pre-flood, indicated groundwater as the main source of riverine input, due to snow cover and frozen topsoil (Dahlqvist et al., 2007; Wortberg et al., 2017). With increasing discharge, the input from organic rich soil layers increased, as shown by the smaller $\delta^{18}O$ signal and an increase in Fe and DOC concentrations accompanied by a decline in pH and conductivity (Laudon et al., 2002; Wu et al., 2016). In forested areas this may be the result of a rising water table leading to a shift in the source from mineral to upper soil layers (Buffam et al., 2007). Post-spring flood levels of all water chemical variables returned towards values observed at base-flow in winter, indicating a higher input of ground water.

We hypothesized that changing hydro-geological pathways would affect Fe speciation in the river water. No significant relationships between Fe speciation and e.g. discharge was found, nevertheless there was a tendency that Fe speciation varied alongside the variables indicative of different source regions. A higher contribution of Fe-OM complexes was found during high flow. Throughout the sampling period, Fe (oxy)hydroxides were strongly dominating. Dahlqvist et al. (2007) proposed that Fe-rich colloids are the predominant phase during winter. Those originate from Fe(II) in anoxic groundwater that is oxidized when reaching the oxic stream water with the subsequent formation of Fe (oxy)hydroxides. In contrast, during high discharge caused by snowmelt, sub-surface run off drains organic-rich soil layers that becomes a source of stream water Fe-OM complexes (Dahlqvist et al., 2007; Grabs et al., 2012; Riedel et al., 2013; Rosenberg and Schroth, 2017).

Interestingly, a minor drop in the contribution of Fe-OM complexes was detected at peak flow. Potentially, this was caused by mobilization of particulate Fe from the riverbanks or the river bed by the massive discharge flushing the system (Withers and Jarvie, 2008; Rosenberg and Schroth, 2017). This is consistent with the importance of particulate matter for Fe transport during high discharge in a boreal river as shown by Björkvald et al. (2008).

Our collective results showed that in all samples Fe(III) was the only oxidation state detected. This is in agreement with other studies on Fe speciation at river mouths (Herzog et al., 2017). Hence, no temporal variability was detected in the oxidation state of Fe at the sampling locations. While Fe(II) may be found in soils and soil pore waters (Sundman et al., 2014) and low order streams (Herzog et al., 2019), the increasing oxygen and pH conditions along the flow path favor oxidation and the predominance of Fe(III) (Neubauer et al., 2013).

4.2. Fe transport capacity and link to speciation

The Fe transport capacity values for the Kalix and Råne River were low compared to previous studies on boreal rivers (Kritzberg et al., 2014; Herzog et al., 2017). These low Fe transport capacities may be linked to the minor contribution of Fe-OM, since the Fe transport capacity has been shown to be positively correlated to the relative contribution of Fe-OM (Herzog, 2018). While no significant correlation between the Fe transport capacity and Fe-OM was detected, a similar temporal pattern was observed. Both Fe transport capacity and the relative contribution of Fe-OM were relatively higher during high discharge. Interestingly, both showed a drop at peak flow. The higher contribution of Fe (oxy)hydroxides, shown by the XAS results, may explain this temporary drop in the Fe transport capacity.

4.3. Link between Fe isotope and Fe speciation

The aggregates formed in response to increasing salinity were completely dominated by Fe (oxy)hydroxides. Thus, these Fe (oxy)hydroxides were selectively removed from suspension in agreement with previous results (Herzog et al., 2017). Interestingly, the aggregates were consistently enriched in the light ^{54}Fe isotope compared to the river water Fe, while the supernatant was consistently enriched in the heavier ^{56}Fe. This suggests that Fe (oxy)hydroxides are isotopically lighter, and Fe-OM complexes, which contributed more to the suspended fraction, are isotopically heavy. This is in line with recent studies that have identified ubiquitously heavy $\delta^{56}Fe$ values in the dissolved fraction (< 0.45 μm) in organic-rich rivers and light $\delta^{56}Fe$ in the larger size fraction (> 0.45 μm) (Escoube et al. 2009, 2015; Ilina et al., 2013). Furthermore, organically complexed Fe(III) is expected to be enriched in the heavy isotope relative to uncomplexed dissolved Fe, since covalent bonds with ^{56}Fe are stronger (Dideriksen et al., 2008). These findings may also explain the positive Fe isotope ratio of the colloidal Fe (1 kda–0.22 μm) found in the outer river plume of the Lena River, while a negative particulate Fe (> 0.22 μm) phase was lost close to the river mouth (Conrad et al., 2019). The aggregation experiment shows that Fe-OM with a positive $\delta^{56}Fe$ ratio, resist the salinity induced mixing, therefore they might reflect the positive $\delta^{56}Fe$ ratio found in the Arctic Ocean.

The river water Fe isotopic composition varied over the sampling period while the XAS analyses revealed a strong dominance of Fe (oxy) hydroxides during the same period, with a tendency to higher contribution of Fe-OM complexes at higher discharge. The $\delta^{56}Fe$ ratio became lighter as discharge increased. Thus, while low $\delta^{56}Fe$ corresponded with predominance of Fe (oxy)hydroxides in the experiments separating aggregates from Fe in suspension, declining river water $\delta^{56}Fe$ was observed when the contribution from Fe-OM complexes was relatively higher. This demonstrates that there is no simple relationship between the river water isotopic composition and Fe speciation.

The river water $\delta^{56}Fe$ correlated with DOC concentrations, conductivity and O isotope signatures, suggesting that the $\delta^{56}Fe$ is affected by the different source areas of Fe and the varying hydrogeological conditions (Escoube et al., 2015; Ingri et al., 2018). Thus, while there are links between $\delta^{56}Fe$ ratios and Fe speciation, numerous processes along the river flow path should affect and alter Fe speciation and cause isotopic fractionation, which implies that $\delta^{56}Fe$ values in the river mouth cannot be assumed to directly reflect Fe speciation of the source region. Notably, the interpretation from our experimental separation – that Fe-OM complexes are isotopically heavier than Fe (oxy)hydroxides, are in line with high $\delta^{56}Fe$ in organic soil layers, and heavier isotopic Fe signatures during increasing discharge in a first-order stream, *i.e.* closer to the source (Ingri et al., 2018).

Since there was little variation in Fe oxidation state and strong dominance of Fe(III) in all samples, variation in $\delta^{56}Fe$ did not reflect differences in oxidation state. The presence of Fe(II) in soils and low-order streams has been previously shown (Sundman et al., 2014), and Ingri et al. (2018) suggested that low $\delta^{56}Fe$ found below the groundwater table, and in stream water at winter base flow, was due to mineral dissolution of Fe(II), which is preferential to the lighter isotope (Brantley et al., 2004). Moreover, along the flow path from the source area, a gradual increase of Fe(III), towards a complete dominance in the river mouth, was observed by Herzog et al. (2019). Thus, while it may be possible to infer Fe oxidation state and mobilization processes of Fe by isotopic signatures close to the source (e.g. the riparian zone), establishing such links far down stream in the river mouth may not be feasible.

5. Conclusions

Fe speciation in the Kalix and Råne River changed over the season with Fe (oxy)hydroxides dominating during pre- and post-flood with an increasing contribution from Fe-OM complexes during spring flood. Still, the contribution from Fe-OM complexes, even during spring flood, was low and consequently all samples were dominated by Fe (oxy)hydroxides. This was reflected in the overall low Fe transport capacity, compared to results from other river systems (Kritzberg et al., 2014).

Though the data showed a seasonal variation in Fe speciation and Fe transport capacity, the variation was considerably less distinct than expected (Andersson et al., 2006; Dahlqvist et al., 2007). An important and interesting future study would be to conduct a similar study on a river system with a higher contribution of Fe-OM complexes. Smaller catchments closer connected to the Fe source regions may provide such conditions, but sampling that encompass seasonal variability would be required to substantiate such a hypothesis. Increasing the spatial resolution along a river course, including first order streams, may help to explain the intricate relationship between Fe sources, aquatic Fe speciation, and Fe isotope signatures. Finally, since salinity induced aggregation showed a separation into isotopically lighter Fe (oxy)hydroxides and isotopically heavier Fe-OM complexes this difference in isotope composition could be used to better understand which Fe species remains in solution along an estuarine transects. This would be informative since a direct assessment of Fe speciation in marine water by XAS is so far not possible.

Acknowledgments

Synchrotron work was conducted at beamline line 4-1 at the Stanford Synchrotron Radiation Lightsource (SSRL), California, USA. Use of the Stanford Synchrotron Radiation Lightsource, SLAC National Accelerator Laboratory, is supported by the U.S. Department of Energy, Office of Science, Office of Basic Energy Sciences under Contract No. DE-AC02-76SF00515. The SSRL Structural Molecular Biology Program is supported by the DOE Office of Biological and Environmental Research, and by the National Institutes of Health, National Institute of General Medical Sciences (including P41GM103393). The contents of this publication are solely the responsibility of the authors and do not necessarily represent the official views of NIGMS or NIH.

Iron isotopic compositions were measured at ALS Scandinavia AB. We thank the Swedish Meteorological and Hydrological Institute (SMHI) for monitoring data of Swedish river. Thanks to Sofia Mebrahtu Wisén for analyzing the samples at the inorganic analytical laboratory. Financial support for this project was provided by the Swedish Research Council (grant number 2015-05450), the Swedish Research Council Formas through the strong research environment Managing the Multiple Stressors of the Baltic Sea (grant number 207-2010-126). This study was further funded by MetTrans, (a European Union Seventh Framework Marie Curie ITN) [Grant No. 290336]. We thank Bio4Energy, a Strategic Research Environment appointed by the Swedish government, for supporting this work.

Appendix A. Supplementary data

Supplementary data to this article can be found online at https://doi.org/10.1016/j.apgeochem.2019.104385.

References

Anbar, A., Jarzecki, A., Spiro, T., 2005. Theoretical investigation of iron isotope fractionation between Fe (H2O) 63+ and Fe (H2O) 62+: implications for iron stable isotope geochemistry. Geochim. Cosmochim. Acta 69, 825–837.

Andersson, K., Dahlqvist, R., Turner, D., Stolpe, B., Larsson, T., Ingri, J., Andersson, P., 2006. Colloidal rare earth elements in a boreal river: changing sources and distributions during the spring flood. Geochim. Cosmochim. Acta 70, 3261–3274.

Ankudinov, A., Ravel, B., Rehr, J., Newville, M., 1992. FEFFIT Manual within the FEFF Project. University of Washington, Seattle, USA **1999**:0.5.

Baxter, D.C., Rodushkin, I., Engström, E., Malinovsky, D., 2006. Revised exponential model for mass bias correction using an internal standard for isotope abundance ratio measurements by multi-collector inductively coupled plasma mass spectrometry. J. Anal. At. Spectrom. 21, 427–430.

Björkvald, L., Buffam, I., Laudon, H., Mörth, C.-M., 2008. Hydrogeochemistry of Fe and Mn in small boreal streams: the role of seasonality, landscape type and scale. Geochim. Cosmochim. Acta 72, 2789–2804.

Björnerås, C., Weyhenmeyer, G.A., Evans, C.D., Gessner, M.O., Grossart, H.P., Kangur, K., Kokorite, I., Kortelainen, P., Laudon, H., Lehtoranta, J., 2017. Widespread increases in iron concentration in European and North American freshwaters. Glob. Biogeochem. Cycles 31, 1488–1500.

Boyd, P.W., Ellwood, M.J., 2010. The biogeochemical cycle of iron in the ocean. Nat. Geosci. 3, 675–682.

Brantley L., S., Liermann J., L., Guynn L., R., Anbar, A., Icopini A., G., Barling, J., 2004. Fe isotopic fractionation during mineral dissolution with and without bacteria. Geochimica et Cosmochimica Acta 68 (15), 3189–3204.

Breitbarth, E., Achterberg, E.P., Ardelan, M., Baker, A.R., Bucciarelli, E., Chever, F., Croot, P., Duggen, S., Gledhill, M., Hassellöv, M., 2010. Iron biogeochemistry across marine systems–progress from the past decade. Biogeosciences 7, 1075–1097.

Buffam, I., Laudon, H., Temnerud, J., Mörth, C.M., Bishop, K., 2007. Landscape-scale variability of acidity and dissolved organic carbon during spring flood in a boreal stream network. J. Geophys. Res.: Biogeosciences 112.

Chester, R., Jickells, T., 2003. The transport of material to the oceans: relative flux magnitudes. Mar. Geochem. 92–124 third ed.

Conrad, S., Ingri, J., Gelting, J., Nordblad, F., Engström, E., Rodushkin, I., Andersson, P.S., Porcelli, D., Gustafsson, Ö., Semiletov, I., 2019. Distribution of Fe isotopes in particles and colloids in the salinity gradient along the Lena River plume, Laptev Sea. Biogeosciences 16, 1305–1319.

Dahlqvist, R., Andersson, K., Ingri, J., Larsson, T., Stolpe, B., Turner, D., 2007. Temporal variations of colloidal carrier phases and associated trace elements in a boreal river. Geochim. Cosmochim. Acta 71, 5339–5354.

Dideriksen, K., Baker, J.A., Stipp, S.L.S., 2008. Equilibrium Fe isotope fractionation between inorganic aqueous Fe (III) and the siderophore complex, Fe (III)-desferrioxamine B. Earth Planet. Sci. Lett. 269, 280–290.

Escoube, R., Rouxel, O.J., Pokrovsky, O.S., Schroth, A., Holmes, R.M., Donard, O.F., 2015. Iron isotope systematics in Arctic rivers. Compt. Rendus Geosci. 347, 377–385.

Escoube, R., Rouxel, O.J., Sholkovitz, E., Donard, O.F., 2009. Iron isotope systematics in estuaries: the case of North River, Massachusetts (USA). Geochim. Cosmochim. Acta 73, 4045–4059.

Fromm, E., 1965. Beskrivning Av Jordartskartan Över Norrbotten Län, Nedanför Lappmarksgränsen (In Swedish with English Summary), vol. 39 SGU Serie CA.

Funke, H., Scheinost, A., Chukalina, M., 2005. Wavelet analysis of extended x-ray absorption fine structure data. Phys. Rev. B 71 094110.

Grabs, T., Bishop, K., Laudon, H., Lyon, S.W., Seibert, J., 2012. Riparian zone hydrology and soil water total organic carbon (TOC): implications for spatial variability and upscaling of lateral riparian TOC exports. Biogeosciences 9, 3901–3916.

Haei, M., Öquist, M.G., Buffam, I., Ågren, A., Blomkvist, P., Bishop, K., Ottosson Löfvenius, M., Laudon, H., 2010. Cold winter soils enhance dissolved organic carbon concentrations in soil and stream water. Geophys. Res. Lett. 37.

Herzog, S.D., 2018. Fate of Riverine Iron over Estuarine Salinity Gradients. Lund University (Thesis).

Herzog, S.D., Kvashnina, K., Persson, P., Kritzberg, E., 2019. Organic iron complexes enhance iron transport capacity along estuarine salinity gradients. Biogeosci. Discuss. 2019, 1–20.

Herzog, S.D., Persson, P., Kritzberg, E.S., 2017. Salinity effects on iron speciation in boreal river waters. Environ. Sci. Technol. 51, 9747–9755.

Ilina, S.M., Poitrasson, F., Lapitskiy, S.A., Alekhin, Y.V., Viers, J., Pokrovsky, O.S., 2013. Extreme iron isotope fractionation between colloids and particles of boreal and temperate organic-rich waters. Geochim. Cosmochim. Acta 101, 96–111.

Ingri, J., Conrad, S., Lidman, F., Nordblad, F., Engström, E., Rodushkin, I., Porcelli, D., 2018. Iron isotope pathways in the boreal landscape: role of the riparian zone. Geochim. Cosmochim. Acta 239, 49–60.

Ingri, J., Malinovsky, D., Rodushkin, I., Baxter, D.C., Widerlund, A., Andersson, P., Gustafsson, Ö., Forsling, W., Öhlander, B., 2006. Iron isotope fractionation in river colloidal matter. Earth Planet. Sci. Lett. 245, 792–798.

Ingri, J., Torssander, P., Andersson, P., Mörth, C.-M., Kusakabe, M., 1997. Hydrogeochemistry of sulfur isotopes in the Kalix River catchment, northern Sweden. Appl. Geochem. 12, 483–496.

Jickells, T.D., An, Z.S., Andersen, K.K., Baker, A.R., Bergametti, G., Brooks, N., Cao, J.J., Boyd, P.W., Duce, R.A., Hunter, K.A., Kawahata, H., Kubilay, N., laRoche, J., Liss, P.S., Mahowald, N., Prospero, J.M., Ridgwell, A.J., Tegen, I., Torres, R., 2005. Global iron connections between desert dust, ocean biogeochemistry, and climate. Science 308, 67–71.

Karlsson, T., Persson, P., 2010. Coordination chemistry and hydrolysis of Fe (III) in a peat humic acid studied by X-ray absorption spectroscopy. Geochim. Cosmochim. Acta 74, 30–40.

Karlsson, T., Persson, P., Skyllberg, U., Mörth, C.-M., Giesler, R., 2008. Characterization of iron (III) in organic soils using extended X-ray absorption fine structure spectroscopy. Environ. Sci. Technol. 42, 5449–5454.

Kester, D.R., Duedall, I.W., Connors, D.N., Pytkowicz, R.M., 1967. Preparation of artificial seawater. Limnol. Oceanogr. 12, 176–179.

Klementev, K., 2001. Statistical evaluations in fitting problems. J. Synchrotron Radiat. 8, 270–272.

Klementiev, K., 2000. VIPER for Windows (Visual Processing in EXAFS Researches). freeware.

Klementiev, K., 2002. XANES Dactyloscope for Windows. KV Klementiev, XANES Dactyloscope for Windows. freeware. www.desy.de/~klmn/xanda.html.

Krachler, R., Krachler, R.F., von der Kammer, F., Suphandag, A., Jirsa, F., Ayromlou, S., Hofmann, T., Keppler, B.K., 2010. Relevance of peat-draining rivers for the riverine input of dissolved iron into the ocean. Sci. Total Environ. 408, 2402–2408.

Kritzberg, E.S., Bedmar Villanueva, A., Jung, M., Reader, H.E., 2014. Importance of boreal rivers in providing iron to marine waters. PLoS One 9 e107500.

Kritzberg, E.S., Ekstrom, S.M., 2012. Increasing iron concentrations in surface waters - a factor behind brownification? Biogeosciences 9, 1465–1478.

Lalonde, K., Mucci, A., Ouellet, A., Gélinas, Y., 2012. Preservation of organic matter in sediments promoted by iron. Nature 483, 198–200.

Laudon, H., Hemond, H.F., Krouse, R., Bishop, K.H., 2002. Oxygen 18 fractionation

during snowmelt: implications for spring flood hydrograph separation. Water Resour. Res. 38.
Ledesma, J.L., Futter, M.N., Blackburn, M., Lidman, F., Grabs, T., Sponseller, R.A., Laudon, H., Bishop, K.H., Köhler, S.J., 2018. Towards an improved conceptualization of riparian zones in boreal forest headwaters. Ecosystems 21, 297–315.
Lenstra, W.K., Egger, M., van Helmond, N.A., Kritzberg, E., Conley, D.J., Slomp, C.P., 2018. Large variations in iron input to an oligotrophic Baltic Sea estuary: impact on sedimentary phosphorus burial. Biogeosciences 15, 6979–6996.
Neal, C., Lofts, S., Evans, C.D., Reynolds, B., Tipping, E., Neal, M., 2008. Increasing iron concentrations in UK upland waters. Aquat. Geochem. 14, 263–288.
Neff, J., Finlay, J., Zimov, S., Davydov, S., Carrasco, J., Schuur, E., Davydova, A., 2006. Seasonal changes in the age and structure of dissolved organic carbon in Siberian rivers and streams. Geophys. Res. Lett. 33.
Neubauer, E., Schenkeveld, W.D., Plathe, K.L., Rentenberger, C., Von Der Kammer, F., Kraemer, S.M., Hofmann, T., 2013. The influence of pH on iron speciation in podzol extracts: iron complexes with natural organic matter, and iron mineral nanoparticles. Sci. Total Environ. 461, 108–116.
Nilsson, M.C., Wardle, D.A., 2005. Understory vegetation as a forest ecosystem driver: evidence from the northern Swedish boreal forest. Front. Ecol. Environ. 3 (8), 421–428.
Nowostawska, U., Kim, J.P., Hunter, K.A., 2008. Aggregation of riverine colloidal iron in estuaries: a new kinetic study using stopped-flow mixing. Mar. Chem. 110, 205–210.
Öquist, M., Laudon, H., 2008. Winter soil frost conditions in boreal forests control growing season soil CO2 concentration and its atmospheric exchange. Glob. Chang. Biol. 14, 2839–2847.
O'day, P.A., Rivera, N., Root, R., Carroll, S.A., 2004. X-ray absorption spectroscopic study of Fe reference compounds for the analysis of natural sediments. Am. Mineral. 89, 572–585.
Peel, M.C., Finlayson, B.L., McMahon, T.A., 2007. Updated world map of the Köppen-Geiger climate classification. Hydrol. Earth Syst. Sci. Discuss. 4, 439–473.
Persson, P., Axe, K., 2005. Adsorption of oxalate and malonate at the water-goethite interface: molecular surface speciation from IR spectroscopy. Geochim. Cosmochim. Acta 69, 541–552.
Pokrovsky, O., Schott, J., Dupré, B., 2006. Trace element fractionation and transport in boreal rivers and soil porewaters of permafrost-dominated basaltic terrain in Central Siberia. Geochim. Cosmochim. Acta 70, 3239–3260.
Riedel, T., Zak, D., Biester, H., Dittmar, T., 2013. Iron traps terrestrially derived dissolved organic matter at redox interfaces. Proc. Natl. Acad. Sci. 110, 10101–10105.
Rosenberg, B.D., Schroth, A.W., 2017. Coupling of reactive riverine phosphorus and iron species during hot transport moments: impacts of land cover and seasonality. Biogeochemistry 132, 103–122.
Sarkkola, S., Nieminen, M., Koivusalo, H., Laurén, A., Kortelainen, P., Mattsson, T., Palviainen, M., Piirainen, S., Starr, M., Finér, L., 2013. Iron concentrations are increasing in surface waters from forested headwater catchments in eastern Finland. Sci. Total Environ. 463–464, 683–689.
Schroth, A.W., Crusius, J., Chever, F., Bostick, B.C., Rouxel, O.J., 2011. Glacial influence on the geochemistry of riverine iron fluxes to the Gulf of Alaska and effects of deglaciation. Geophys. Res. Lett. 38.
Sholkovitz, E., 1976. Flocculation of dissolved organic and inorganic matter during the mixing of river water and seawater. Geochim. Cosmochim. Acta 40, 831–845.
Stumm, W., Morgan, J., 1996. Chemical equilibria and rates in natural waters. Aquat. Chem. 521–531.
Sunda, W.G., Huntsman, S.A., 1997. Interrelated influence of iron, light and cell size on marine phytoplankton growth. Nature 390, 389–392.
Sundman, A., Karlsson, T., Laudon, H., Persson, P., 2014. XAS study of iron speciation in soils and waters from a boreal catchment. Chem. Geol. 364, 93–102.
Tagliabue, A., Bowie, A.R., Boyd, P.W., Buck, K.N., Johnson, K.S., Saito, M.A., 2017. The integral role of iron in ocean biogeochemistry. Nature 543, 51.
Taylor, S., 1964. Trace element abundances and the chondritic Earth model. Geochim. Cosmochim. Acta 28, 1989–1998.
Webb, S., 2005. SIXpack: a graphical user interface for XAS analysis using IFEFFIT. Phys. Scr. 2005, 1011.
Weyhenmeyer, G.A., Prairie, Y.T., Tranvik, L.J., 2014. Browning of boreal freshwaters coupled to carbon-iron interactions along the aquatic continuum. PLoS One 9 e88104.
Wilke, M., Farges, F., Petit, P.-E., Brown, G.E., Martin, F., 2001. Oxidation state and coordination of Fe in minerals: an Fe K-XANES spectroscopic study. Am. Mineral. 86, 714–730.
Withers, P., Jarvie, H., 2008. Delivery and cycling of phosphorus in rivers: a review. Sci. Total Environ. 400, 379–395.
Wojdyr, M., 2010. Fityk: a general-purpose peak fitting program. J. Appl. Crystallogr. 43, 1126–1128.
Wortberg, K., Conrad, S., Andersson, P.S., Ingri, J., 2017. Strontium isotopes–A tracer for river suspended iron aggregates. Appl. Geochem. 79, 85–90.
Wu, J.-k., Ding, Y.-j., Yang, J.-h., Liu, S.-w., Chen, J.-z., Zhou, J.-x., Qin, X., 2016. Spatial variation of stable isotopes in different waters during melt season in the Laohugou Glacial Catchment, Shule River basin. J. Mt. Sci. 13, 1453–1463.
Zabinsky, S., Rehr, J., Ankudinov, A., Albers, R., Eller, M., 1995. Multiple-scattering calculations of X-ray-absorption spectra. Phys. Rev. B 52, 2995.